Chemical Science

ROYAL SOCIETY OF CHEMISTRY

EDGE ARTICLE

View Article Online
View Journal | View Issue

Cite this: *Chem. Sci.*, 2021, **12**, 9408

All publication charges for this article have been paid for by the Royal Society of Chemistry

Molecular design of thermally activated delayed fluorescent emitters for narrowband orange–red OLEDs boosted by a cyano-functionalization strategy†

Yang Liu, Xin Xiao, You Ran, Zhengyang Bin * and Jingsong You

Received 13th April 2021
Accepted 7th June 2021

DOI: 10.1039/d1sc02042k

rsc.li/chemical-science

The establishment of a simple molecular design strategy to realize red-shifted emission while maintaining good color purity for multi-resonance induced thermally activated delayed fluorescent (MR-TADF) materials remains an appealing yet challenging task. Herein, we demonstrate that the attachment of a cyano (CN) functionality at the lowest unoccupied molecular orbital location of the MR-TADF skeleton can promote attractive red-shifted emission due to the exceptional electron-withdrawing capacity of the CN group, which represents the first example of orange–red MR-TADF emitters. Meanwhile, the linear CN group adopts a coplanar conformation with the MR-framework to restrict structure relaxation associated with rotation, which is beneficial to maintain a small full-width at half-maximum and thus a good color purity. The **CNCz-BNCz**-based OLED device, which utilizes a TADF sensitized mechanism to accelerate the up-conversion process of triplet excitons in the emitting layer, exhibits an outstanding external quantum efficiency (EQE) as high as 33.7%, representing the state-of-the-art performance for orange–red TADF-OLEDs.

Introduction

Organic light-emitting diodes (OLEDs) have attracted a great deal of research effort since the pioneer work reported in 1987 by C. W. Tang and co-workers, and have nowadays been successfully used in flat panel displays.[1] In the industrialization process of OLEDs, phosphorescent OLEDs play a crucial role because of the relatively high device external quantum efficiency (EQE) compared with that of fluorescent OLEDs.[2] In 2011, pure organic thermally activated delayed fluorescent (TADF) materials, which have small singlet–triplet energy gaps (ΔE_{ST}) so as to efficiently upconvert triplet to singlet excitons and potentially achieve 100% exciton utilization, were firstly utilized in OLEDs by Adachi and co-workers.[3] Since then, TADF materials have become a hot research topic in the display field. To acquire a small ΔE_{ST} in an organic compound, a small overlap between the highest occupied molecular orbital (HOMO) and lowest unoccupied molecular orbital (LUMO) distributions is always required according to the principle of quantum mechanics, and can be attainable in the molecular structures containing a spatially separated electron-rich donor (D) and electron-deficient acceptor (A).[4] The intramolecular charge-transfer (ICT) characteristic in the twisted D–A structure provides the TADF material the advantage of easily achieved full-color emission, and thus a large number of TADF materials have been developed in the past decade.[5] However, the twisted D–A molecular structures inevitably cause significant vibronic coupling between the ground state (S_0) and the excited singlet state (S_1) as well as remarkable structure relaxation of S_1.[6] Consequently, TADF materials have broad emission spectra with a full-width at half-maximum (FWHM) as large as 100 nm, which cannot satisfy the requirement of high color purity in high-resolution displays.[5b,7]

Recently, to suppress emission broadening while maintaining the TADF characteristic, a rigid π-conjugated skeleton containing an electron-rich nitrogen (N) atom and electron-deficient boron (B) atom was developed by Hatakeyama and co-workers in 2016.[8] The multi-resonance (MR) effect of nitrogen and boron atoms induces the localization of frontier molecular orbitals (FMOs), which significantly reduces the broadening of emission bands and thus enables excellent color purity.[9] However, the realization of red-shifted emission for MR-induced TADF (MR-TADF) materials is intrinsically difficult because of the rigid heterocyclic structure, and thus MR-TADF materials have flourished only in the emission color of the blue region.[6b,10] Recently, the twisted D–A molecular structure in the MR-skeleton has been introduced to develop green (519 nm)

Key Laboratory of Green Chemistry and Technology of Ministry of Education, College of Chemistry, Sichuan University, 29 Wangjiang Road, Chengdu 610064, People's Republic of China. E-mail: binzhengyang@scu.edu.cn

† Electronic supplementary information (ESI) available: Experimental procedures, spectroscopic data of the compounds and crystallographic data. CCDC 2058430 (**CNCz-BNCz**). For ESI and crystallographic data in CIF or other electronic format see DOI: 10.1039/d1sc02042k

and yellow (549 nm) MR-TADF materials, while the fusion of an additional MR-skeleton *via para* B–π–B and N–π–N linkage has been proven to be an effective method to realize a red (615 nm) MR-TADF material.[9c,f] Notably, although the integration of ICT-induced emission in a twisted D–A structure and MR-induced emission is considered as a promising way to finely tune the emission colors of MR-TADF materials, it would inevitably lead to emission broadening owing to the increased structure relaxation associated with the twisted D–A structure. For example, **BCz-BN** with a purely MR-induced emission characteristic displays a blue emission (481 nm) with a small FWHM of 22 nm,[11] while ***m*-Cz-BNCz** that features an auxiliary carbazole group on the HOMO distribution exhibits a green emission (519 nm) with an increased FWHM of 38 nm.[9c] Therefore, the realization of red-shifted emission for MR-TADF materials without sacrificing color purity remains an appealing yet challenging task.

In this work, we wish to represent a cyano (CN)-functionalization strategy to provide red-shifted emission while maintaining good color purity in the MR-TADF skeleton (Fig. 1). Based on FMO engineering, we propose that the electron-withdrawing CN group located on the LUMO distribution could decrease the LUMO energy level to lead to red-shifted emission (Fig. S1†),[12] and meanwhile adopt a coplanar conformation with the MR-skeleton to restrict structure relaxation associated with rotation, which is beneficial to maintain a small FWHM. As a result, a CN functionality, introduced on a blue-emitting MR-TADF skeleton (**BCz-BN**), leads to a 15 nm red-shifted emission with a small FWHM of 21 nm for **CN-BCz-BN** (Fig. 1 and S2†), while a CN functionality, introduced on a yellow-emitting MR-TADF skeleton (**BBCz-Y**), gives a more significant red-shifted emission of 32 nm and maintains a relatively small FWHM of 42 nm (**CNCz-BNCz**, Fig. 1), which represents the first example of orange–red MR-TADF emitters.[6b,8–11]

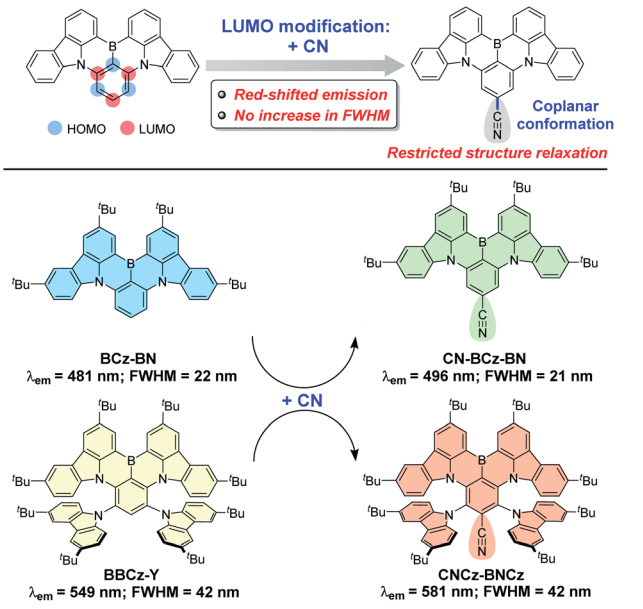

Fig. 1 Molecular design concept and the summary of molecular structures, emission wavelengths and FWHMs of **BCz-BN**, **BBCz-Y**, **CN-BCz-BN** and **CNCz-BNCz**.

Results and discussion

The synthetic route to **CNCz-BNCz** is illustrated in Scheme 1 (for **CN-BCz-BN**, see Scheme S2†). Starting from commercially available 1,4-dibromotetrafluorobenzene (**1**), the multiple nucleophilic aromatic substitution reactions were conducted to deliver compound **2** in 95% yield. Subsequently, the boron atom was incorporated to construct the key precursor **3** through an electrophilic borylation reaction. Finally, a transnitrilation reaction with dimethylmalononitrile (DMMN) furnished the target molecule **CNCz-BNCz**.[13] **CNCz-BNCz** was purified by column chromatography, recrystallization from dichloromethane/methanol and finally temperature gradient vacuum sublimation as a red solid. The thermogravimetric analysis revealed a good thermal stability with a decomposition temperature of 409 °C (T_d, the temperature for 5% weight loss) for the vacuum deposition process (Fig. S3a†). The single crystals of **CNCz-BNCz** for X-ray crystallographic analysis were obtained *in situ* during the temperature gradient vacuum sublimation process (Scheme 1 and Table S1†).[14] The C–C bond length from the carbon position of the CN group to the *para*-carbon position of the B-substituted phenyl-ring is 1.443 Å, indicative of the double-bond character. As predicted, the CN group adopts a coplanar conformation with the MR-skeleton, which can inhibit structure relaxation and potentially maintain a small FWHM.

The photophysical properties of **CNCz-BNCz** were measured and are summarized in Fig. 2 and Table S2.† The UV-vis absorption spectrum exhibits an intense absorption band with an absorption peak at 547 nm, which is attributed to the strong ICT absorption transition. In toluene, the fluorescence spectrum (Fl.) measured at room temperature displays a strong orange–red fluorescence emission with an emission peak at 581 nm. A relatively small Stokes shift of 34 nm reveals a small

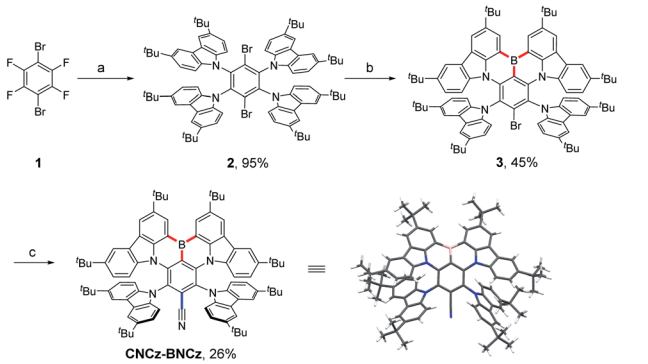

Scheme 1 Synthetic route to **CNCz-BNCz**. Reaction conditions: (a) (i) *tert*-butylcarbazole, NaH, *N*,*N*-dimethylformamide, rt, 0.5 h; (ii) 1,4-dibromotetrafluorobenzene, 140 °C, 12 h. (b) (i) *n*-BuLi, toluene, −60 °C, 1 h; (ii) BBr_3, −40 °C to 0 °C, 1 h; (iii) $EtN(i\text{-}Pr)_2$, 120 °C, 8 h. (c) (i) *n*-BuLi, tetrahydrofuran, −78 °C, 1 h; (ii) dimethylmalononitrile (DMMN), −78 °C to rt, overnight. Inset: the crystal structure of **CNCz-BNCz**.

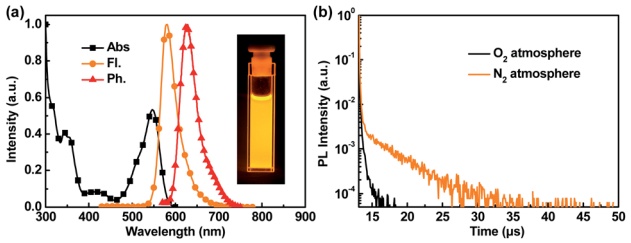

Fig. 2 (a) Absorption spectrum (Abs.), fluorescence spectrum (Fl.), and phosphorescence spectrum (Ph.) of **CNCz-BNCz** in toluene solution at 1×10^{-5} mol L^{-1} under ambient conditions. (b) Transient photoluminescence spectra of **CNCz-BNCz** in toluene solution at 1×10^{-5} mol L^{-1} under an O_2 atmosphere and N_2 atmosphere, respectively.

molecular conformation change between the ground state and the excited state, which leads to a small FWHM of 42 nm. Compared with **BBCz-Y**, **CNCz-BNCz** exhibits a significant red-shifted emission from 549 nm to 581 nm, but can maintain the same FWHM of 42 nm in toluene solution (Fig. 2a and S2†).

Furthermore, a significant solvatochromic effect was observed in different solvents, which indicates the strong ICT properties of **CNCz-BNCz** (Fig. S4†). As shown in Fig. S5 and S6,† when the concentration of **CNCz-BNCz** is increased, the Fl. spectra display similar emission bands with slightly red-shifted emission peaks, while the Abs. spectra exhibit the same absorption peaks. It demonstrates that there might not exist significant pi–pi dimerization of **CNCz-BNCz** and the effect of excimers may be negligible.[15,16]

In toluene solution at 10^{-5} mol L^{-1}, the singlet energy (E_{S1}) of 2.28 eV is calculated from the onset wavelength of the Fl. spectrum, while the triplet energy (E_{T1}) of 2.10 eV is calculated from the onset wavelength of the phosphorescence (Ph.) spectrum measured at 77 K, indicating a ΔE_{ST} value of 0.18 eV (Fig. 2a). The Fl. and Ph. spectra are also measured in 3 wt% doped-polystyrene film at different temperatures (Fig. S7†). The ΔE_{ST} values are almost identical at temperatures ranging from 77 K to 157 K, revealing a negligible decrease in the conjugation of the lowest triplet state.[16] Furthermore, the emission of CNCz-BNC in polystyrene film red shifts by 22 meV from room temperature (298 K) to low temperature (77 K), which indicates that hot vibrational excited states contribute to radiative decay at room temperature (Fig. S8†).[16]

The TADF nature of **CNCz-BNCz** was further investigated by transient photoluminescent spectra. As shown in Fig. 2b, the transient photoluminescent spectrum in toluene solution under a N_2 atmosphere exhibits an obviously delayed component, indicating a significant TADF characteristic of **CNCz-BNCz**. Benefiting from the MR-effect, the radiative decay rate (k_r) of **CNCz-BNCz** is as high as 2.2×10^7 s^{-1} (Table S3†). Similar to other MR-TADF materials, **CNCz-BNCz** has a relatively small reverse intersystem crossing rate (k_{RISC}) of 4.2×10^5 s^{-1} (Table S3†).

With an efficient orange–red MR-TADF emitter in hand (Tables S2 and S3†), we tried to assemble high-performance OLED devices. Prior to device fabrication, the HOMO energy level is obtained from cyclic voltammetry measurement, while the LUMO energy level is calculated from the HOMO energy

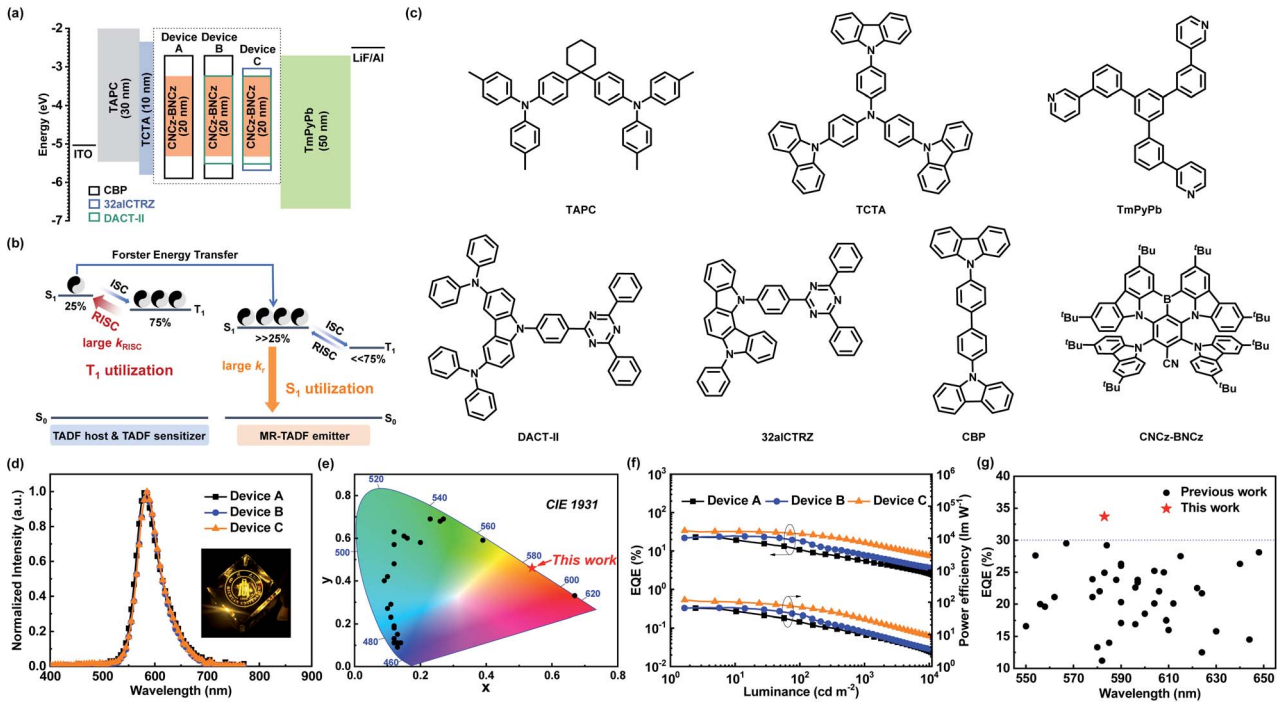

Fig. 3 (a) Device structures and energy level diagrams of devices A, B and C. (b) Energy transfer process from the TADF host and TADF sensitizer to the MR-TADF emitter. (c) Molecular structures used in OLED devices. (d) EL spectra at the luminance of 1000 cd m^{-2}. (e) Color coordinates of device C on CIE 1931 color space compared with the other B–N based MR-TADF materials reported. (f) EQE and power efficiency *versus* luminance curves of OLED devices. (g) EQE_{max} summary of TADF-OLEDs with an emission peak from 550 to 650 nm.

Table 1 Summary of EL characteristics for OLED devices

Device	EL_{peak} [nm]	V_{on}[a] [V]	FWHM [nm]	EQE_{max}[b] [%]	PE_{max}[c] [lm W^{-1}]	CIE[d] [x, y]	At 100 cd m^{-2} EQE [%]	At 100 cd m^{-2} PE [lm W^{-1}]	At 1000 cd m^{-2} EQE [%]	At 1000 cd m^{-2} PE [lm W^{-1}]
A	584	3.3	49	23.0	65.4	[0.55, 0.45]	10.8	24.8	5.4	9.6
B	584	3.1	50	24.7	67.4	[0.53, 0.45]	17.7	38.3	7.8	11.7
C	583	2.7	49	33.7	117.8	[0.54, 0.46]	27.7	69.1	16.4	29.6

[a] Turn-on voltage. [b] External quantum efficiency. [c] Power efficiency. [d] Commission Internationale de l'Eclairage (CIE) coordinates.

level and the optical bandgap measured from the absorption spectrum, which are −5.33 eV and −3.19 eV, respectively (Fig. S3b†). Doped in the widely used *N*,*N*-dicarbazolyl-4,4′-biphenyl (CBP) host, **CNCz-BNCz** exhibits outstanding orange–red emission with absolute photoluminescence quantum yields (Φ_{PL}) as high as 96% and FWHM as small as 45 nm (Fig. S9 and Table S4†). The optimized device structures and energy transfer processes are described in Fig. 3a and b, and the molecular structures used in OLEDs are shown in Fig. 3c. 4,4′-Cyclohexylidenebis[*N*,*N*-bis(4-methylphenyl)aniline] (TAPC) and 1,3,5-tri[(3-pyridyl)-phen-3-yl]benzene (TmPyPb) are used as the hole transporting material and electron transporting material, respectively. A thin layer of 4,4′,4″-tris(carbazol-9-yl)-triphenylamine (TCTA) was introduced to confine excitons. The OLED performances are shown in Fig. 3d–g and S10 and S11† and summarized in Tables 1 and S5.†

As reported, OLEDs based on MR-TADF emitters (MR-TADF OLEDs) can achieve outstanding EL efficiency with superior color purity and excellent EQE_{max} because of extremely high k_r (10^7–10^8 s^{-1}).[6b,9c,9f] However, their relatively small k_{RISC} (10^4–10^5 s^{-1}) compared with those of ICT induced TADF materials (10^6–10^7 s^{-1}) would lead to severe triplet–triplet annihilation in the emitting layer (EML).[17] Consequently, the MR-TADF OLEDs usually suffer from significant efficiency roll-off. For example, the EQE_{max} of device A, which utilizes 3% of **CNCz-BNCz** as an emitter in a conventional CBP host in the EML, is 23.0% at 1.7 cd m^{-2}, but when the luminance is increased to 100 and 1000 cd m^{-2}, the EQEs rapidly drop to 10.8% (EQE_{100}) and 5.4% (EQE_{1000}). Then we utilized a TADF-sensitized mechanism to suppress the efficiency roll-off by integrating the advantages of high k_r for MR-TADF emitters and high k_{RISC} for ICT-TADF hosts. Subsequently, we used a ternary system containing an additional TADF sensitizer (DACT-II) in the **CNCz-BNCz**:CBP doped EML to assist the up-conversion process of triplet excitons. Based on this method, device B displays a comparable EQE_{max} of 24.7% with a reduced efficiency roll-off (EQE_{100} of 17.7%). Nevertheless, the efficiency roll-off at 1000 cd m^{-2} is still serious with an EQE_{1000} of 7.8%. In device C, the traditional CBP host is replaced by an efficient TADF host (32aICTRZ) to further accelerate the triplet exciton dynamics in the EML.[18] Intriguingly, device C exhibits an outstanding EL performance with a record-high EQE_{max} of 33.7% and a significantly reduced efficiency roll-off (EQE_{100} of 27.7%; EQE_{1000} of 16.4%) (Fig. 3g and S12, and Table S6†). Moreover, the balanced hole–electron bipolar transporting properties of TADF host 32aICTRZ[18] endow device C with a low turn-on voltage of 2.7 V and thus a considerably high power efficiency of 117.8 lm W^{-1}, which is approximately twice as high as those of devices A and B utilizing a conventional CBP host (65.4 lm W^{-1} for device A; 67.4 lm W^{-1} for device B).

Conclusions

In conclusion, we have designed and synthesized an orange–red emitting MR-TADF material, **CNCz-BNCz**, by attaching a linear CN group on a yellow-emitting **BBCz-Y** MR-skeleton. **CNCz-BNCz** exhibits a narrowband emission with a high Φ_{PL} of 90% and a fast k_r as high as 2.2×10^7 s^{-1}, which can enable the efficient emitter in TADF sensitized-OLEDs for the simultaneous realization of good color purity, high EQE with low efficiency roll-off and high power efficiency. This work not only offers a new approach for the future development of full-color MR-TADF materials, but also exemplifies the great potential of the TADF-sensitized mechanism in assembling high-performance OLED devices.

Author contributions

Y. Liu carried out most parts of the experiments. X. Xiao and Y. Ran synthesized some of the materials. Z. Bin and J. You supervised the project. All authors contributed to the discussion of the results.

Conflicts of interest

There are no conflicts to declare.

Acknowledgements

We acknowledge financial support from the National NSF of China (No. 22031007 and 22005204) and the Sichuan Science and Technology Program (No. 2020YJ0245 and 2020YJ0302). We also thank the Comprehensive Training Platform Specialized Laboratory, College of Chemistry, Sichuan University.

Notes and references

1 C. W. Tang and S. A. VanSlyke, *Appl. Phys. Lett.*, 1987, **51**, 913–915.
2 M. A. Baldo, M. E. Thompson and S. R. Forrest, *Nature*, 2000, **403**, 750.

3 H. Uoyama, K. Goushi, K. Shizu, H. Nomura and C. Adachi, *Nature*, 2012, **492**, 234.

4 (*a*) Y.-J. Shiu, Y.-C. Cheng, W.-L. Tsai, C.-C. Wu, C.-T. Chao, C.-W. Lu, Y. Chi, Y.-T. Chen, S.-H. Liu and P.-T. Chou, *Angew. Chem., Int. Ed.*, 2016, **55**, 3017–3021; (*b*) X.-L. Chen, J.-H. Jia, R. Yu, J.-Z. Liao, M.-X. Yang and C.-Z. Lu, *Angew. Chem., Int. Ed.*, 2017, **56**, 15006–15009; (*c*) J. Huang, H. Nie, J. Zeng, Z. Zhuang, S. Gan, Y. Cai, J. Guo, S.-J. Su, Z. Zhao and B. Z. Tang, *Angew. Chem., Int. Ed.*, 2017, **56**, 12971–12976; (*d*) I. S. Park, K. Matsuo, N. Aizawa and T. Yasuda, *Adv. Funct. Mater.*, 2018, **28**, 1802031; (*e*) Z. Huang, Z. Bin, R. Su, F. Yang, J. Lan and J. You, *Angew. Chem., Int. Ed.*, 2020, **59**, 9992–9996; (*f*) W. Liang, Y. Yang, M. Yang, M. Zhang, C. Li, Y. Ran, J. Lan, Z. Bin and J. You, *Angew. Chem., Int. Ed.*, 2021, **60**, 3493–3497; (*g*) L. Wu, K. Wang, C. Wang, X.-C. Fan, Y.-Z. Shi, X. Zhang, S.-L. Zhang, J. Ye, C.-J. Zheng, Y.-Q. Li, J. Yu, X.-M. Ou and X.-H. Zhang, *Chem. Sci.*, 2021, **12**, 1495–1502.

5 (*a*) M. Y. Wong and E. Zysman-Colman, *Adv. Mater.*, 2017, **29**, 1605444; (*b*) Y. Im, M. Kim, Y. J. Cho, J.-A. Seo, K. S. Yook and J. Y. Lee, *Chem. Mater.*, 2017, **29**, 1946–1963; (*c*) Z. Yang, Z. Mao, Z. Xie, Y. Zhang, S. Liu, J. Zhao, J. Xu, Z. Chi and M. P. Aldred, *Chem. Soc. Rev.*, 2017, **46**, 915–1016; (*d*) Y. Liu, C. Li, Z. Ren, S. Yan and M. R. Bryce, *Nat. Rev. Mater.*, 2018, **3**, 18020; (*e*) D.-H. Kim, A. D'Aléo, X.-K. Chen, A. D. S. Sandanayaka, D. Yao, L. Zhao, T. Komino, E. Zaborova, G. Canard, Y. Tsuchiya, E. Choi, J. W. Wu, F. Fages, J.-L. Brédas, J.-C. Ribierre and C. Adachi, *Nat. Photonics*, 2018, **12**, 98–104; (*f*) T.-L. Wu, M.-J. Huang, C.-C. Lin, P.-Y. Huang, T.-Y. Chou, R.-W. Chen-Cheng, H.-W. Lin, R.-S. Liu and C.-H. Cheng, *Nat. Photonics*, 2018, **12**, 235–240; (*g*) X. Liang, Z.-L. Tu and Y.-X. Zheng, *Chem.–Eur. J.*, 2019, **25**, 5623–5642; (*h*) D. H. Ahn, S. W. Kim, H. Lee, I. J. Ko, D. Karthik, J. Y. Lee and J. H. Kwon, *Nat. Photonics*, 2019, **13**, 540–546; (*i*) R. Su, Y. Zhao, F. Yang, L. Duan, J. Lan, Z. Bin and J. You, *Sci. Bull.*, 2021, **66**, 441–448.

6 (*a*) F. Santoro, A. Lami, R. Improta, J. Bloino and V. Barone, *J. Chem. Phys.*, 2008, **128**, 224311; (*b*) Y. Kondo, K. Yoshiura, S. Kitera, H. Nishi, S. Oda, H. Gotoh, Y. Sasada, M. Yanai and T. Hatakeyama, *Nat. Photonics*, 2019, **13**, 678–682.

7 X. Li, Y.-Z. Shi, K. Wang, M. Zhang, C.-J. Zheng, D.-M. Sun, G.-L. Dai, X.-C. Fan, D.-Q. Wang, W. Liu, Y.-Q. Li, J. Yu, X.-M. Ou, C. Adachi and X.-H. Zhang, *ACS Appl. Mater. Interfaces*, 2019, **11**, 13472–13480.

8 T. Hatakeyama, K. Shiren, K. Nakajima, S. Nomura, S. Nakatsuka, K. Kinoshita, J. Ni, Y. Ono and T. Ikuta, *Adv. Mater.*, 2016, **28**, 2777–2781.

9 (*a*) Y. Zhang, D. Zhang, J. Wei, Z. Liu, Y. Lu and L. Duan, *Angew. Chem., Int. Ed.*, 2019, **58**, 16912–16917; (*b*) N. Ikeda, S. Oda, R. Matsumoto, M. Yoshioka, D. Fukushima, K. Yoshiura, N. Yasuda and T. Hatakeyama, *Adv. Mater.*, 2020, **32**, 2004072; (*c*) Y. Xu, C. Li, Z. Li, Q. Wang, X. Cai, J. Wei and Y. Wang, *Angew. Chem., Int. Ed.*, 2020, **59**, 17442–17446; (*d*) Y. Zhang, D. Zhang, J. Wei, X. Hong, Y. Lu, D. Hu, G. Li, Z. Liu, Y. Chen and L. Duan, *Angew. Chem., Int. Ed.*, 2020, **59**, 17499–17503; (*e*) S. Oda, W. Kumano, T. Hama, R. Kawasumi, K. Yoshiura and T. Hatakeyama, *Angew. Chem., Int. Ed.*, 2021, **60**, 2882–2886; (*f*) M. Yang, I. S. Park and T. Yasuda, *J. Am. Chem. Soc.*, 2020, **142**, 19468–19472.

10 (*a*) X. Liang, Z.-P. Yan, H.-B. Han, Z.-G. Wu, Y.-X. Zheng, H. Meng, J.-L. Zuo and W. Huang, *Angew. Chem., Int. Ed.*, 2018, **57**, 11316–11320; (*b*) K. Matsui, S. Oda, K. Yoshiura, K. Nakajima, N. Yasuda and T. Hatakeyama, *J. Am. Chem. Soc.*, 2018, **140**, 1195–1198; (*c*) S. H. Han, J. H. Jeong, J. W. Yoo and J. Y. Lee, *J. Mater. Chem. C*, 2019, **7**, 3082–3089; (*d*) S. Oda, B. Kawakami, R. Kawasumi, R. Okita and T. Hatakeyama, *Org. Lett.*, 2019, **21**, 9311–9314.

11 Y. Xu, Z. Cheng, Z. Li, B. Liang, J. Wang, J. Wei, Z. Zhang and Y. Wang, *Adv. Opt. Mater.*, 2020, **8**, 1902142.

12 (*a*) D. G. Congrave, B. H. Drummond, P. J. Conaghan, H. Francis, S. T. E. Jones, C. P. Grey, N. C. Greenham, D. Credgington and H. Bronstein, *J. Am. Chem. Soc.*, 2019, **141**, 18390–18394; (*b*) Y.-L. Zhang, Q. Ran, Q. Wang, Y. Liu, C. Hänisch, S. Reineke, J. Fan and L.-S. Liao, *Adv. Mater.*, 2019, **31**, 1902368; (*c*) T. Yang, Z. Cheng, Z. Li, J. Liang, Y. Xu, C. Li and Y. Wang, *Adv. Funct. Mater.*, 2020, **30**, 2002681; (*d*) K. Zheng, F. Ni, Z. Chen, C. Zhong and C. Yang, *Angew. Chem., Int. Ed.*, 2020, **59**, 9972–9976.

13 J. T. Reeves, C. A. Malapit, F. G. Buono, K. P. Sidhu, M. A. Marsini, C. A. Sader, K. R. Fandrick, C. A. Busacca and C. H. Senanayake, *J. Am. Chem. Soc.*, 2015, **137**, 9481–9488.

14 ESI†

15 M. K. Etherington, N. A. Kukhta, H. F. Higginbotham, A. Danos, A. N. Bismillah, D. R. Graves, P. R. McGonigal, N. Haase, A. Morherr, A. S. Batsanov, C. Pflumm, V. Bhalla, M. R. Bryce and A. P. Monkman, *J. Phys. Chem. C*, 2019, **123**, 11109–11117.

16 K. Stavrou, A. Danos, T. Hama, T. Hatakeyama and A. Monkman, *ACS Appl. Mater. Interfaces*, 2021, **13**, 8643–8655.

17 C. Bohne, E. B. Abuin and J. C. Scaiano, *J. Am. Chem. Soc.*, 1990, **112**, 4226–4231.

18 D. Zhang, X. Song, M. Cai, H. Kaji and L. Duan, *Adv. Mater.*, 2018, **30**, 1705406.